

# Four Changing-Look Active Galactic Nuclei Found From Optical Variations

Li-Tao Zhu<sup>1</sup>, Jie Li<sup>2,3</sup>, Zhongxiang Wang<sup>1,4,\*</sup>, Ju-Jia Zhang<sup>5,6</sup>

<sup>1</sup>*Department of Astronomy, School of Physics and Astronomy, Yunnan University, Kunming 650091, China; wangzx20@ynu.edu.cn*

<sup>2</sup>*Laboratory for Research in Galaxies and Cosmology, Department of Astronomy, University of Science and Technology of China, Hefei 230036, China*

<sup>3</sup>*School of Astronomy and Space Science, University of Science and Technology of China, Hefei 230026, China*

<sup>4</sup>*Shanghai Astronomical Observatory, Chinese Academy of Sciences, Shanghai 200030, China*

<sup>5</sup>*Yunnan Observatories, Chinese Academy of Sciences, Kunming 650216, China*

<sup>6</sup>*Key Laboratory for the Structure and Evolution of Celestial Objects, Chinese Academy of Sciences, Kunming 650216, China*

Accepted XXX. Received YYY; in original form ZZZ

## ABSTRACT

We report the finding of four changing-look (CL) active galactic nuclei (AGN). We selected these sources due to their potential as interesting targets when considering their relatively-large optical flux variations and related mid-infrared flux variations. To identify their CL feature, we use archival spectra from the Sloan Digital Sky Survey (SDSS) taken at least 8 years ago as well as spectra taken recently from the Transient Name Server (TNS) and with the 2.4-m LiJiang telescope (LJT). We study the sources' spectral changes by fitting and determining the  $H_\alpha$  and  $H_\beta$  components and verify their CL behavior. When comparing the TNS and/or LJT spectra to the SDSS ones, all four sources showed the appearance of a broad or a stronger broad  $H_\alpha$  component and a relatively weak broad  $H_\beta$  component. As two of the four sources are established to have a brighter-and-bluer feature in the photometric data, during the time periods in which the TNS and LJT spectra were taken, this feature likely accompanied the turn-on of the broad components. Thus, we suggest that this brighter-and-bluer feature can be used as a criterion for efficiently finding CL sources among previously spectroscopically classified type 2 AGN, such as from among the sources provided by the SDSS.

**Key words:** galaxies: active — quasars: emission lines

## 1 INTRODUCTION

According to the framework of the unification scheme for Active Galactic Nuclei (AGN), they can be classified into two types, type 1 and type 2, depending on our viewing angle of the galactic central region that contains the power source, an actively accreting supermassive black hole (SMBHs; e.g., Lawrence 1987; Antonucci 1993; Urry & Padovani 1995; Tadhunter 2008). For type 1, broad ( $\gtrsim 1000 \text{ km s}^{-1}$ ) and narrow ( $\leq 1000 \text{ km s}^{-1}$ ) emission lines are seen in optical or ultraviolet (UV) spectra as we are viewing the centers with low inclination angles, while for type 2, only narrow lines can be seen since the broad line regions (BLRs), presumably closer to the centers than the narrow line regions (NLRs), are obscured by the dusty tori that surround the SMBHs. This unification scheme has worked well in understanding of various AGN phenomena but is now being challenged by the so-called Changing-Look AGN (CLAGN) discovered in recent years.

CLAGN can be identified from either X-ray or optical/UV spectroscopy. In X-rays, the majority of the CLAGN can

be seen to have undergone transitions between Compton-thick and Compton-thin states (e.g., Matt et al. 2003; Puccetti et al. 2007; Bianchi et al. 2009; Risaliti et al. 2009; Marchese et al. 2012; see also Ricci & Trakhtenbrot 2022 and references therein). The transitions, intricately linked to the levels of obscuration, are possibly attributed to various causes, such as eclipses, fluctuations in the ionization state of the obscuring gas, outflows, or the switching on-and-off of the central engine.

In optical (and UV) wavelengths, occasional cases of striking appearances or disappearances of broad emission lines (BELs), in particular a pronounced  $H_\beta$  component, have been reported in early years (e.g., Tohline & Osterbrock 1976; Cohen et al. 1986; Storchi-Bergmann et al. 1993; Aretxaga et al. 1999; Eracleous & Halpern 2001; Denney et al. 2014; Shappee et al. 2014). This includes the first quasar case (LaMassa et al. 2015). Because of the intriguing features and their importance in helping further reveal the physical processes in AGN, systematic searches for CLAGN have recently been conducted given the advent of rich data from different surveys. As a result, an increasing number of CLAGN have been reported (e.g., Ruan et al.

\* E-mail: wangzx20@ynu.edu.cn

2016; MacLeod et al. 2016; Yang et al. 2018; Sheng et al. 2020; Green et al. 2022).

The methods performed in these searches were to compare the spectra from different epochs all the while taking into consideration flux variations, since spectral changes were notably accompanied with large flux variations (see, e.g., López-Navas et al. 2023b and references therein). We have been working on studies of  $\sim 40$  AGN flux-variation cases, selected mainly from the optical imaging survey data from the Zwicky Transient Facility (ZTF; Bellm et al. 2019), and have found them showing different interesting patterns (e.g., Li, Wang & Zheng 2023). Most of these AGN have archival spectra from the Sloan Digital Sky Survey (SDSS; Abazajian et al. 2009), and by comparing that with the spectra reported at the Transient Name Server (TNS) and/or spectra obtained by us with the 2.4-m LiJiang Telescope (LJT; Wang et al. 2019), we were able to identify four CLAGN among them. They are named as J0113+0135, J1127+3546, J1223+0645, and J1513+1759 (hereafter J0113, J1127, J1223, and J1513, respectively). Information for them is provided in Table 1. We note also that one of them, J0113, has already been reported by López-Navas et al. (2022) as a CLAGN.

In this paper, we report the results that lead to the identification of the four CLAGN. In Section 2, we describe the optical and infrared (IR) photometric and spectroscopic data we used in the studies; as we conducted spectroscopic observations ourselves for three of them, we also provide the details of our observations and data reductions. The spectrum results and analysis, which show the changing-look (CL) feature of the four sources, are presented in Section 3. Finally we discuss the results in Section 4, where we also point out that a brightness-color behavior of AGN could be a key criterion for efficiently selecting CLAGN candidates. Throughout this paper, we adopted cosmological parameters from the Planck mission (Planck Collaboration et al. 2020), with  $H_0 = 67 \text{ km s}^{-1} \text{ Mpc}^{-1}$ .

## 2 DATA AND OBSERVATIONS

### 2.1 Archival Data

In order to find AGN with significant flux variations, we mainly used the ZTF  $g$ - and  $r$ -band ( $zg$  and  $zr$  respectively) data. Magnitudes of the two bands are in the AB photometric system (Bellm et al. 2019), similar to those (Medford et al. 2020) provided in the Panoramic Survey Telescope and Rapid Response System (Chambers et al. 2016). We required catflags = 0 and  $chi < 4$  when querying ZTF data to be able to construct a clean and good-quality light curve for a source, and when interesting sources were found, we added other available photometric data in order to obtain as complete a light curve as was possible at multiple bands. The other data included were cyan (420–650 nm;  $ac$ ) and orange (560–820 nm;  $ao$ ) bands, where the two cover the SDSS filters  $g+r$  and  $r+i$  wavelength ranges respectively, from the Asteroid Terrestrial-impact Last Alert System (ATLAS; Tonry et al. 2018),  $V$  band (Vega based system) from the Catalina Real-Time Transient Survey (CRTS; Drake et al. 2009), and mid-IR (MIR) W1 (3.4  $\mu\text{m}$ ) and W2 (4.6  $\mu\text{m}$ ) bands from the Post-Cryo survey of the Wide field Infrared Survey Explorer (WISE; Wright et al. 2010).

**Table 1.** Source information for the four CLAGN

Source	R.A. (J2000)	Decl. (J2000)	$z$	Mag <sup>a</sup>
J0113	01 <sup>h</sup> 13 <sup>m</sup> 11 <sup>s</sup> .8	+01°35′42″.5	0.24	19.23
J1127	11 <sup>h</sup> 27 <sup>m</sup> 59 <sup>s</sup> .3	+35°46′44″.8	0.075	17.78
J1223	12 <sup>h</sup> 23 <sup>m</sup> 10 <sup>s</sup> .6	+06°45′54″.9	0.24	17.99
J1513	15 <sup>h</sup> 13 <sup>m</sup> 20 <sup>s</sup> .9	+17°59′16″.1	0.13	17.01

<sup>a</sup> Magnitudes were ZTF  $g$ -band values at the times of the most recent spectroscopic observations, except for J1513+1759 whose ATLAS  $ao$  value is given.

**Table 2.** Information for spectroscopic observations with LJT

Target	Date	Seeing ( $''$ )	Exposure (sec)	Standard
J0113	2022-10-20	0.75	2400	BD+33d2642
J1223	2022-04-23	1.46	1500	Feige110
J1513	2023-05-07	1.03	1800	BD+33d2642

All four sources have an optical spectrum from the SDSS database, while three of the four have an spectrum each from the TNS database; J0113 was reported by Pellegrino et al. (2022), J1127 by Jacobson-Galán & Foley (2021), and J1513 by Hinkle (2022). We also obtained spectra ourselves for three of the AGN for purposes of either confirmation or identification; the spectroscopic observation details are described in the following Section 2.2.

### 2.2 LJT observations

Using the LJT, we conducted spectroscopic observations of three of the sources. The Yunnan Faint Object Spectrograph and Camera (YFOSC), whose detector is a  $2048 \times 4096$  pixel<sup>2</sup> back-illuminated CCD with a pixel scale of  $0.283'' \text{ pixel}^{-1}$ , was used for spectroscopy. In all exposures, a G3 grism was chosen, providing a wavelength coverage of 340–910 nm and a spectral dispersion of  $0.29 \text{ nm pixel}^{-1}$ . A long slit with a width of  $2.5''$  was chosen for all exposures. Along with each of the exposures of the sources, spectra of a He-Ne lamp and a spectrophotometric standard were also taken for the wavelength and flux calibration, respectively. Information for the observations, which includes the date, seeing, exposure time, and standard star, are given in Table 2.

Using the IRAF tasks, the spectrum-image data were processed by performing bias-subtraction and flat-fielding. Spectra of the sources were then extracted, with wavelength and flux calibrations conducted.

## 3 ANALYSIS AND RESULTS

Visual inspection of the spectra of the four AGN taken at different epochs suggested the presence of the CL feature. We employed the Python QSO fitting code (PyQSOFit; Guo et al. 2018) to obtain measurements on the key emission lines,  $H_\alpha$  and  $H_\beta$  in the spectra. From the spectral fitting, the full-width at half maximum (FWHM), equivalent width (EW), and line flux for each of the two lines were obtained. In addition, the peak wavelength for each line’s broad component was also obtained. The results are given in Table 3, and the fitting details are presented in Figures A1–A4 in Section Appendix A.

However for the results, two caveats should be taken into

consideration. The first is the line broadening due to the seeing or the slit width. Because the SDSS and TNS spectra are the archival data, we only estimated the effect in our LJT observations. Since the seeing was smaller than the slit width in the exposures, the broadening due to the former approximately had  $\text{FWHM}_{\text{seeing}} \simeq 7.7, 15.0, \text{ and } 10.6 \text{ \AA}$  for the LJT spectra of J0113, J1223, and J1513 (cf., Table 2), respectively. The corresponding values in units of kilometer per second at the observed  $\text{H}_\beta$  ( $\text{H}_\alpha$ ) line are approximately 380, 750, and 570 (280, 550, and 420), respectively. These  $\text{FWHM}_{\text{seeing}}$  should be subtracted from FWHMs given in Table 3 in quadrature, and they can reduce the FWHMs of the narrow lines upto  $\sim 23\%$ , while they obviously do not significantly affect the FWHMs of the broad lines.

The second is the uncertainties on the spectra, which should be dominated by systematic ones. To estimate them, we checked the fluxes of several continuum regions of a TNS or LJT spectrum that have a roughly same flux level but different noise levels. The average flux difference with respect to that of the continuum region of the lowest noise was considered as the systematic uncertainty of a spectrum. The uncertainties estimated this way are approximately 10%, 9%, and 17% for the LJT spectra of J0113, J1223, and J1513, respectively, and 6%, 3%, and 9% for the TNS spectra of J0113, J1127, and J1513, respectively. These uncertainties should be considered as the systematic ones to the measurements of the line features given in Table 3.

### 3.1 J0113+0135

This source had a flat  $V$ -band light curve in the past, but its ZTF light curves show a  $\sim -0.5$  mag rise after MJD 59000. The MIR W1 and W2 light curves also show an accompanying rise, appearing to have lasted longer than the optical rise (Figure 1). Broad emission lines are clearly visible when comparing the spectrum from the TNS (taken near the peak of the rise) with the SDSS spectrum (taken on MJD 57282), and the broad-line feature was still present in our LJT spectrum (taken on MJD 59872), when the optical light curves were already turning downwards. The spectral fitting results indicate that the broad  $\text{H}_\alpha$  and  $\text{H}_\beta$  components had FWHMs of  $\sim 5000\text{--}6000 \text{ km s}^{-1}$ . The redshift value was determined to be  $\simeq 0.24$ . Following Vestergaard & Peterson (2006), the mass of the SMBH  $M_{\text{BH}}$  was estimated from

$$\log\left(\frac{M_{\text{BH}}}{M_\odot}\right) = \log\left[\left(\frac{\text{FWHM}(\text{H}_\beta)}{\text{km s}^{-1}}\right)^2 \left(\frac{L_{5100}}{10^{44} \text{ erg s}^{-1}}\right)^{0.5}\right] + 0.91, \quad (1)$$

where  $L_{5100}$  is the luminosity at  $5100 \text{ \AA}$ . The mass is  $\sim 10^{8.2} M_\odot$  based on the LJT measurement (Table 3).

As there was a significantly larger/faster flux rise in the blue  $zg$  band, clearly shown in Figure 1, we further checked the details regarding it. A  $zg - zr$  color diagram, derived in approximation from the data points of  $zg$  and  $zr$  taken within one day, is shown in Figure 2. Initially at  $\sim 1.0$  mag, the color decreases, reaching to as low as  $\sim 0.5$  mag before rising back to  $\sim 0.75$  mag at the time when the LJT spectrum was taken. In addition, we found that the color changes follow a brighter-and-bluer pattern,  $zg - zr \propto 0.59zr$ . The magnitude-color diagram showing the derived relationship is presented in Figure B1 in Appendix B.

Unfortunately, no spectra were taken right before the color change at MJD 59000, so we do not know if the CL feature occurred in tandem with the change or not. It is interesting to see that the MIR fluxes also increased, with magnitude changes of  $\sim -1$  mag in both W1 and W2 bands, and that it did not follow the flux fallback seen in the optical variations. We did not conduct tests to determine the correlation behavior between the optical and MIR bands, such as, checking if there were any time delays in the MIR flux increases with respect to the optical rise, since the simple light-curve shapes (as well as the sparse data points in the MIR bands) would be unlikely to provide definitive results.

### 3.2 J1127+3546

This source also had a flat  $V$ -band light curve in the past, but appears to have become highly variable in more recently optical light curves (Figure 3). In particular, at the observation of the TNS spectrum, its  $zg$  and  $zr$  appeared to have risen by  $\sim -0.5$  mag, similarly seen in the ATLAS  $ac$  and  $ao$  light curves. The SDSS spectrum taken approximately 18 years ago shows the presence of a broad (but relatively faint)  $\text{H}_\alpha$  component, while the absence of a similar  $\text{H}_\beta$  component (Table 3; see also Figure A2). This type of the spectrum suggests the possibility of the source being a Seyfert 1.8 Galaxy, according to those characteristics outlined in Caccianiga et al. (2008). Then based on the TNS spectrum reported by Pellegrino et al. 2022, the source was classified as a Seyfert 1 Galaxy, since both  $>2500 \text{ km s}^{-1}$  FWHM  $\text{H}_\alpha$  and  $\text{H}_\beta$  components were detected. In addition, the  $\text{H}_\alpha$  component appeared much stronger than that in the SDSS spectrum. Using the TNS spectrum,  $M_{\text{BH}}$  was estimated to be  $\sim 10^{7.2} M_\odot$ .

We also constructed a  $zg - zr$  color diagram for the source, which is shown in Figure 4. As can be seen, the color values have a large spread in the range of 1.0–0.6. Thus, this source not only showed large optical flux variations but also large color variations. Although there is a large spread in values, we tested to fit the colors as a function of  $zr$ , and obtained  $zg - zr \propto 0.2zr$ . However, this possible correlation is weak, as the Spearman’s rank correlation coefficient is only 0.2 (corresponding to a  $p$ -value of 0.8%). By comparison, the coefficient for the correlation in J0113 (and J1223 below) is 0.61 (0.74).

It would be interesting to know what characteristics the spectrum of this source had at the start of the ZTF light curves, where the large flux and color variations occurred. Additionally, a small rise, with magnitude changes of  $\sim -0.2$ , can also be seen in the MIR bands at the time when the TNS spectrum was taken.

### 3.3 J1223+0645

Overall, the variation features of this source, as seen in its multi-band light curves, appear similar to those of J0113. However, different from J0113, the CRTS  $V$ -band light curve of this source also shows variations. Approximately from MJD 58200, the ZTF light curves have a  $\sim -1$  mag rise before reaching the maximum, at which point our LJT spectrum was taken. The MIR fluxes accompanied the optical rise. The SDSS spectrum for comparison was taken nearly 18 years ago. While a weak, broad  $\text{H}_\alpha$  component was required

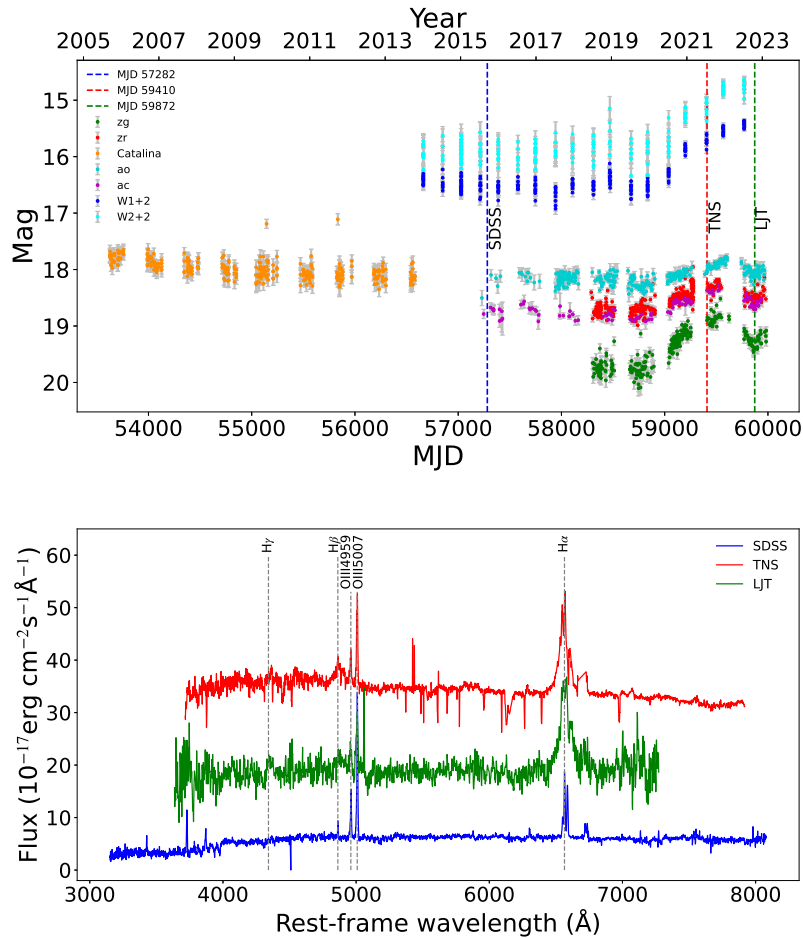


**Figure 1.** Optical and MIR light curves (*top panel*) and optical spectra (*bottom panel*) of J0113+0135. The spectrum taking times are marked by the dashed lines in the top panel. In the bottom panel, the spectra are shifted vertically for clarity, and the key emission lines are indicated.

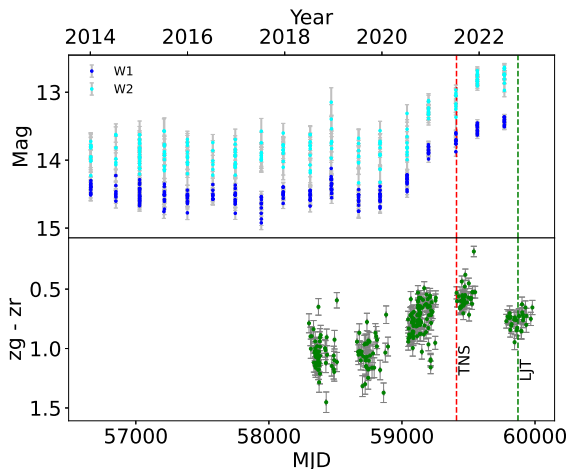


**Figure 2.** *Bottom:*  $z_g - z_r$  color variations of J0113+0135. The dashed lines mark the TNS and LJT spectra taking times. *Top:* Detailed view of the MIR W1 and W2 light curves of the source.

in the fitting of the SDSS spectrum (Table 3; Figure A3), our LJT spectrum shows a similarly broad but significantly stronger  $H_\alpha$  component. The key difference that reveals the

CL feature is the broad  $H_\beta$  component, as no such a component was seen in the SDSS spectrum. Based on the LJT spectrum,  $M_{\text{BH}}$  was estimated to be  $\sim 10^{8.8} M_\odot$ .

A  $z_g - z_r$  color diagram was constructed to show the color changes, as the  $z_g$  light curve had a faster rise than the  $z_r$  one (Figure 6). For this source, excluding two obvious outliers (which were likely real changes due to large  $z_g$  magnitude changes, checked by us on the images and the data points), the color values rise at a constant rate of  $-3.94 \pm 0.10 \times 10^{-4} \text{ mag day}^{-1}$ , reaching a maximum before MJD 59500. After the maximum, our LJT spectrum was taken (see Figure 6). A brighter-and-bluer pattern can also be well established, with  $z_g - z_r \propto 0.36 z_r$  (see Figure B1). Similar to J0113, the MIR fluxes increased during the optical-rise time period, and the magnitude changes were  $\sim -0.5$ .

### 3.4 J1513+1759

This source's  $V$ -band light curve appears flat and with little variation, but after MJD 57000, both the optical and MIR light curves show significant variations. Because there were only a few data points from ZTF, only ATLAS *ac* and *ao* light curves are shown in Figure 7. The TNS spectrum, taken on MJD 59680, shows the detection of a broad  $H_\alpha$  component as

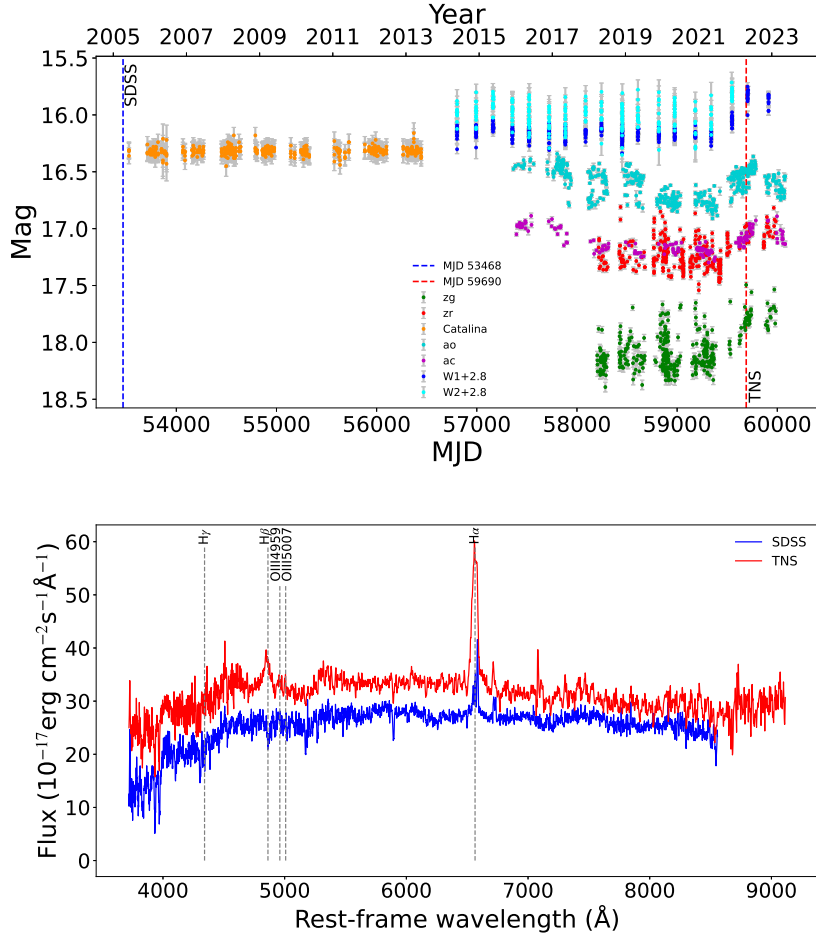


**Figure 3.** Same as Figure 1 for J1127+3546.

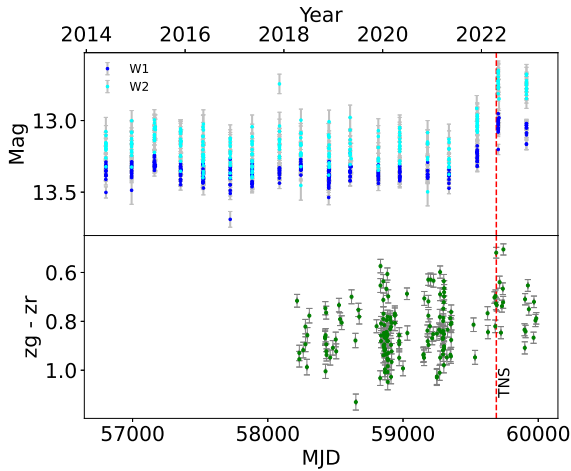


**Figure 4.** Same as Figure 2 for J1127+3546. The dashed line marks the TNS spectrum taking time.

well as the weak detection of a broad  $H_{\beta}$  component (Table 3; Figure A4). In contrast to the SDSS spectrum taken  $\sim 15$  yr ago that does not show any broad components, the newly detected features indicate the CL behavior of the source. It should be noted that at the time the TNS spectrum was taken, the optical light curves were at a local variation peak.

Our LJT spectrum was taken  $\sim 1$  yr later, when the optical light curves reverted to a lower brightness level, but it still contains the broad  $H_{\alpha}$  component. A broad  $H_{\beta}$  was not detected, but the absence of the component could be due to the low signal-to-noise detection of the source spectrum.

We did not construct a color diagram for the optical variations of this source, since the ATLAS bands are much wider than typically used ones (Tonry et al. 2018).

## 4 DISCUSSION

Selecting significantly variable AGN from the ZTF as well as the ATLAS survey data, we have found four sources with the CL feature by comparing the spectra from the archival data and our own targeted spectroscopic observations. In the respective time periods wherein significant flux variations occurred, the spectra of the sources show the appearance of a broad  $H_{\alpha}$  (in the cases of J0113 and J1513) or a stronger one (in the cases of J1127 and J1223). Most of the spectra also show the appearance of a broad, but relatively weak,  $H_{\beta}$  component.

For J0113, López-Navas et al. (2022) have identified it as a CLAGN, and the TNS and LJT spectra in this work have confirmed their identification. Their spectrum was taken at  $\sim$ MJD 59520, in between those of the TNS and LJT and

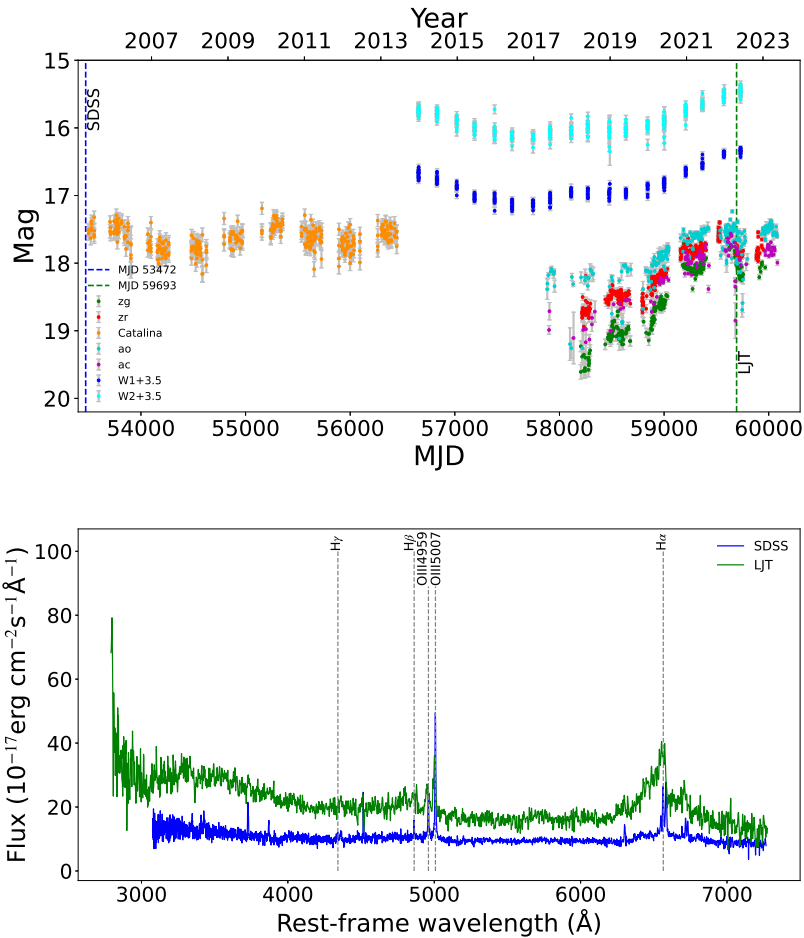


**Figure 5.** Same as Figure 1 for J1223+0645.

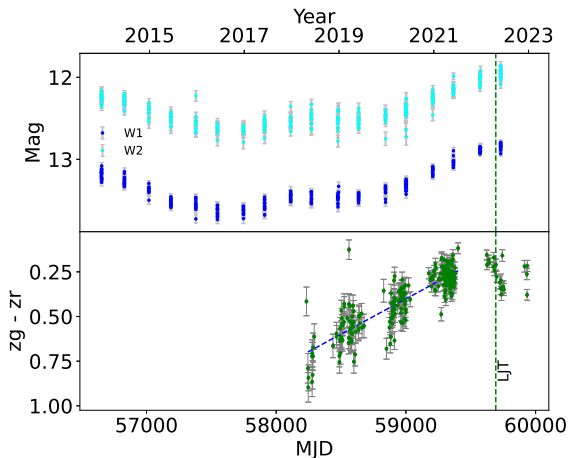


**Figure 6.** Same as Figure 2 for J1223+0645. The vertical dashed line marks the LJT spectrum taking time. In addition, a rate of  $-3.94 \times 10^{-4} \text{ mag day}^{-1}$  (marked by the blue dashed line in the bottom panel) can be derived for the data points approximately before MJD 59500.

around the peak of the optical rise. The broad  $H_{\beta}$  component in their spectrum appeared to be stronger than that in the TNS or LJT spectrum, which is probably not a co-

incidence and likely has physical connections. For J1513, although the TNS and LJT spectra are not of good quality, the absence of a broad  $H_{\beta}$  in the SDSS spectrum, as well as its possible appearance and re-absence in the TNS and LJT spectra, show a similarity to those CL cases such as Mrk 590 (Denney et al. 2014), Mrk 1018 (McElroy et al. 2016), and in particular NGC 4156 (Tozzi et al. 2022). In addition to the appearance of a broad  $H_{\alpha}$  component in 2019, NGC 4156 was found to have a relatively weak, broad  $H_{\beta}$  component, one that weakened further in 2022. The possible weakening of the broad  $H_{\beta}$  component in J1513 occurred over a  $\sim 400$  day period, which is marked by the TNS and LJT spectra.

Another notable feature found in the four AGN is the MIR brightening that accompanied the respective optical flux increase (or variations in J1513). It has been found that this could be a common feature of CL activity (Sheng et al. 2017) and may be used as an indicator for finding CLAGN (Sheng et al. 2020).

The origin of the CL phenomena remains enigmatic. However, the correlated MIR variations can often help exclude the variable obscuration, one broad category of the scenarios often discussed for the CL phenomena, as the cause (Sheng et al. 2017; Ross et al. 2018; Stern et al. 2018). On the other hand, detailed studies of several CL cases have been able to limit potential causes to some physical processes or changes, such as the state transition (which has

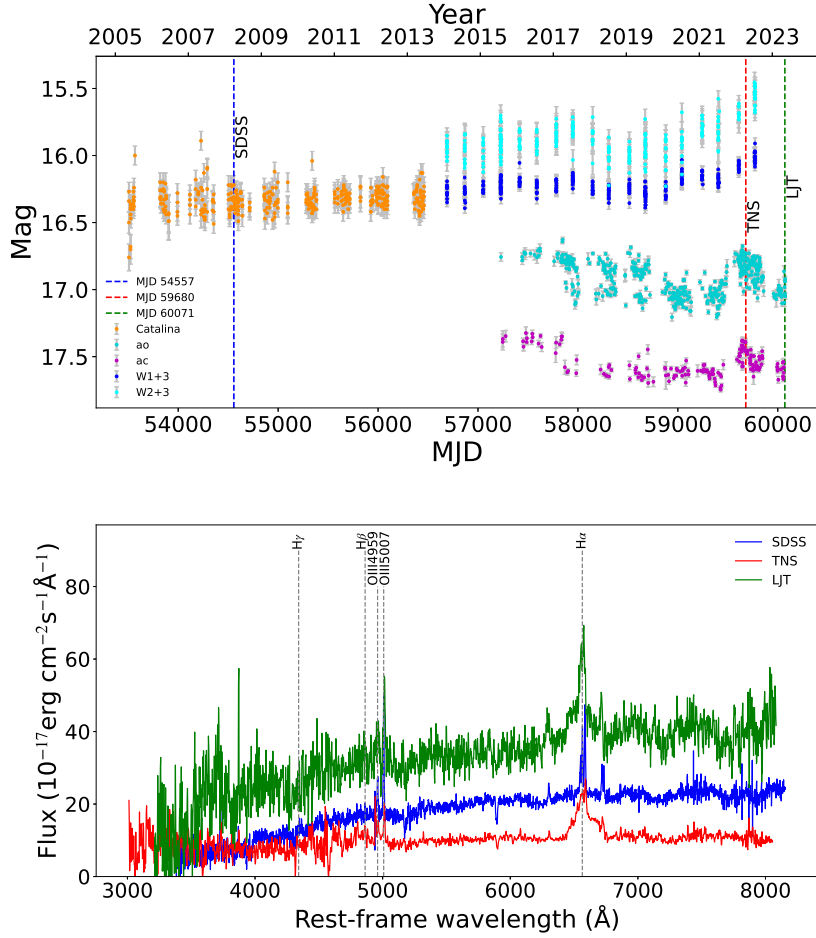


Figure 7. Same as Figure 1 for J1513+1759.

been well studied in black-hole X-ray binaries; Noda & Done 2018; Ai et al. 2020) or disk instabilities (Ross et al. 2018; Stern et al. 2018; Sniegowska et al. 2020) in the inner part of the accretion gas, which is another broad category of the possible scenarios. Because of the comparatively short timescales (months to years) of CL transitions, the process-occurring regions are thus likely small and close to the SMBHs (e.g., Stern et al. 2018; Sniegowska et al. 2020).

Related to the second category of the possibilities, it is conceivable to observe the flux variations that accompany CL transitions, maybe especially in cases demonstrating a change from type 2 to type 1, as the physical processes that could induce the transitions would naturally produce significant optical flux variations. Taking our four cases as an example, they were previously classified as type 2 based on the SDSS spectra, but their relatively large flux variations attracted our attention to carry out follow-up studies. Moreover, for two of them, we have found a brighter-and-bluer feature, one that is commonly seen in type 1 AGN (see Ruan et al. 2014 and references therein). Thus, we suspect that this brightness-color feature could be used as a criterion for finding CL sources.

To roughly test this possibility, we collected a large number of type 2 AGN among the SDSS sources and checked their magnitude-color behavior, although it should be noted that the classifications might not be reliable and could contain many complicated cases (see, e.g., López-Navas et al.

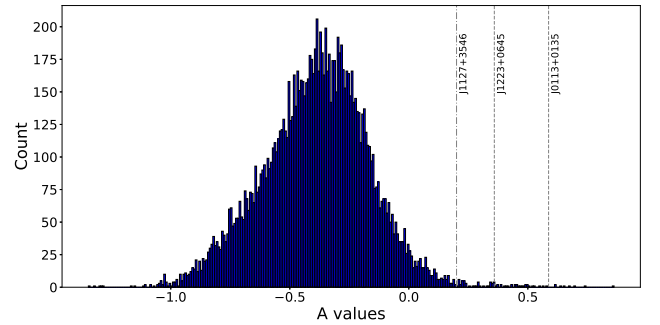


Figure 8.  $k$ -value distribution for 12614 SDSS type 2 AGN. The values for two of the four sources in this work are marked by vertical dashed lines. The value for the weak correlation in J1127 is also marked, with a dash-dotted line.

2023a). We found 12614 SDSS type 2 AGN with ZTF data points greater than 43 in each of the  $zg$  and  $zr$  bands, where we required the median signal-to-noise ratio  $\text{snmedian} \geq 10$  and redshift  $z \leq 0.5$  when querying the SDSS database (details will be reported elsewhere in L. Zhu et al., in preparation). Sources with too few ZTF data points were excluded because sparse data points do not allow us to build a clear magnitude-color relationship. We then fit  $zg - zr$  colors (obtained from the measurements within one day) as a function

**Table 3.** Measurements from fitting the spectra with PyQSOFit

Line	(J0113) SDSS	TNS	LJT	(J1127) SDSS	TNS
<b>H<math>\alpha</math> broad</b>					
FWHM	0	5885 $\pm$ 106	5956 $\pm$ 157	5146 $\pm$ 384	2889.4 $\pm$ 9.2
EW	0	153.5 $\pm$ 1.6	165.6 $\pm$ 3.8	233 $\pm$ 19	447 $\pm$ 10
Flux	0	3900 $\pm$ 41	1647 $\pm$ 38	337 $\pm$ 26	1038 $\pm$ 24
Peak	0	6549.5 $\pm$ 1.1	6569.2 $\pm$ 1.5	6552 $\pm$ 5.0	6556.98 $\pm$ 0.49
<b>H<math>\alpha</math> narrow</b>					
FWHM	443.0 $\pm$ 6.2	551 $\pm$ 21	709 $\pm$ 35	394 $\pm$ 17	826 $\pm$ 14
EW	20.84 $\pm$ 0.49	13.0 $\pm$ 0.68	17.4 $\pm$ 1.3	33.7 $\pm$ 4.4	113.9 $\pm$ 5.0
Flux	162.1 $\pm$ 3.8	331 $\pm$ 17	172 $\pm$ 13	49.3 $\pm$ 6.5	266 $\pm$ 12
<b>H<math>\beta</math> broad</b>					
FWHM	0	5642.5 $\pm$ 2.1	4656 $\pm$ 293	0	2526 $\pm$ 61
EW	0	37.4 $\pm$ 0.9	20.2 $\pm$ 1.9	0	36.98 $\pm$ 0.85
Flux	0	1169 $\pm$ 28	240 $\pm$ 22	0	297.8 $\pm$ 6.8
<b>H<math>\beta</math> narrow</b>					
FWHM	495.9 $\pm$ 9.7	578 $\pm$ 59	991 $\pm$ 57	—	319 $\pm$ 50
EW	3.91 $\pm$ 0.48	1.83 $\pm$ 0.53	1.83 $\pm$ 0.91	—	1.90 $\pm$ 0.69
Flux	30.4 $\pm$ 3.7	57 $\pm$ 17	22 $\pm$ 11	—	15.1 $\pm$ 5.5
MJD	57282	59410	59872	53468	59690
$\log(M_{BH}/M_{\odot})$	—	8.63 $^{+0.06}_{-0.07}$	8.23 $^{+0.12}_{-0.13}$	—	7.18 $\pm$ 0.03
Line	(J1223) SDSS	LJT	(J1513) SDSS	TNS	LJT
<b>H<math>\alpha</math> broad</b>					
FWHM	11973 $\pm$ 3333	14125 $\pm$ 2350	0	8872 $\pm$ 571	8189 $\pm$ 62
EW	82.9 $\pm$ 8.1	274.4 $\pm$ 5.3	0	1141 $\pm$ 43	413.0 $\pm$ 3.0
Flux	970 $\pm$ 94	6237 $\pm$ 120	0	1728 $\pm$ 64	2105 $\pm$ 15
Peak	6548 $\pm$ 19	6507 $\pm$ 17	0	6551.1 $\pm$ 2.2	6547.93 $\pm$ 0.83
<b>H<math>\alpha</math> narrow</b>					
FWHM	392 $\pm$ 14	855 $\pm$ 168	264 $\pm$ 10	604 $\pm$ 75	722.6 $\pm$ 7.4
EW	15.03 $\pm$ 0.97	15.4 $\pm$ 1.0	147.9 $\pm$ 4.7	46.6 $\pm$ 6.9	54.12 $\pm$ 0.79
Flux	176 $\pm$ 11	351 $\pm$ 23	97.0 $\pm$ 3.1	71 $\pm$ 11	276.0 $\pm$ 4.0
<b>H<math>\beta</math> broad</b>					
FWHM	0	7311 $\pm$ 1032	0	5599.6 $\pm$ 5.1	0
EW	0	50.02 $\pm$ 0.81	0	87.2 $\pm$ 3.2	0
Flux	0	1262 $\pm$ 20	0	390 $\pm$ 15	0
<b>H<math>\beta</math> narrow</b>					
FWHM	392 $\pm$ 13	1206 $\pm$ 419	473.1 $\pm$ 7.5	818 $\pm$ 125	972 $\pm$ 15
EW	4.02 $\pm$ 0.18	6.6 $\pm$ 2.6	23.1 $\pm$ 4.8	9.4 $\pm$ 3.1	91.8 $\pm$ 2.7
Flux	1.0 $\pm$ 2.3	130.0 $\pm$ 4.0	23.3 $\pm$ 4.8	41 $\pm$ 13	116.8 $\pm$ 3.4
MJD	53472	59693	54557	59680	60071
$\log(M_{BH}/M_{\odot})$	—	8.75 $^{+0.16}_{-0.18}$	—	8.45 $^{+0.19}_{-0.23}$	—

Notes. 1) Full Width at Half Maximum (FWHM), Equivalent Width (EW), flux, and peak measurements are in units of  $\text{km s}^{-1}$ , angstrom ( $\text{\AA}$ ),  $10^{-17} \text{ erg cm}^{-2} \text{ s}^{-1}$ , and angstrom ( $\text{\AA}$ ), respectively. 2) Approximate systematic uncertainties of 6%, 3%, and 9% for the TNS spectra of J0113, J1127, and J1513, respectively, and 10%, 9%, and 17% for the LJT spectra of J0113, J1223, and J1513, respectively, should be considered for the measurements of the line features. 3) The systematic uncertainties are included to estimate the black hole masses.

of  $zr$ ,  $zg - zr \propto k \times zr$ , where  $k$  is the slope. The distribution of the obtained  $k$  values is shown in Figure 8. As can be seen, different from two of our cases, whose  $k$  values are also indicated in Figure 8, most of the sources in the sample we collected have  $k$  values smaller than 0, which implies that they probably had a brighter-and-redder behavior in the ZTF data. In addition, we also checked sources with  $k \geq 0.1$ . There are 177 of them, among which 10 have already been reported to display the CL phenomena. Thus, we suggest that this color-changing behavior can likely be used for finding BEL-on CLAGN among the recorded type 2 AGN. For example, sources with  $k > 0$  in Figure 8 could be candidate CL sources. A spectroscopy survey of them will reveal if the color-changing behavior could be a key in efficiently finding CLAGN among these previously SDSS spectroscopically classified type 2 AGN.

## ACKNOWLEDGEMENTS

We thank referee for comments that help improve our work. This work was based on observations obtained with the Samuel Oschin Telescope 48-inch and the 60-inch Telescope at the Palomar Observatory as part of the Zwicky Transient Facility project. ZTF is supported by the National Science Foundation under Grant No. AST-2034437 and a collaboration including Caltech, IPAC, the Weizmann Institute for Science, the Oskar Klein Center at Stockholm University, the University of Maryland, Deutsches Elektronen-Synchrotron and Humboldt University, the TANGO Consortium of Taiwan, the University of Wisconsin at Milwaukee, Trinity College Dublin, Lawrence Livermore National Laboratories, and IN2P3, France. Operations are conducted by COO, IPAC, and UW.

This work made use of data products from the Wide-field

Infrared Survey Explorer, which is a joint project of the University of California, Los Angeles, and the Jet Propulsion Laboratory/California Institute of Technology, funded by the National Aeronautics and Space Administration.

This research is supported by the Basic Research Program of Yunnan Province No. 202201AS070005, the National Natural Science Foundation of China (12273033), and the Original Innovation Program of the Chinese Academy of Sciences (E085021002).

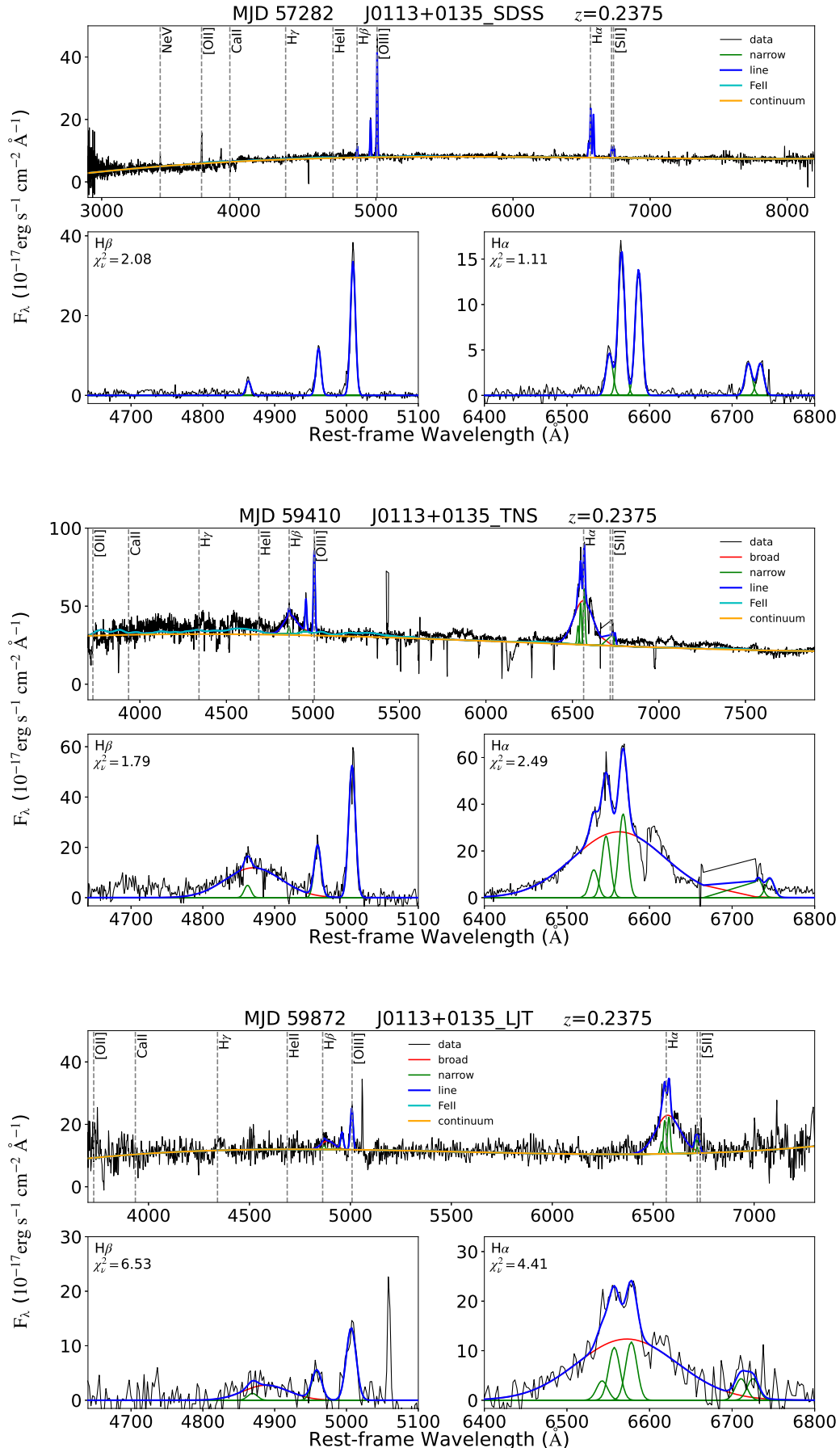
## DATA AVAILABILITY

The data underlying this article will be shared on reasonable request to the corresponding author.

## REFERENCES

- Abazajian K. N., et al., 2009, *ApJS*, **182**, 543  
 Ai Y., et al., 2020, *ApJ*, **890**, L29  
 Antonucci R., 1993, *ARA&A*, **31**, 473  
 Aretxaga I., Joguet B., Kunth D., Melnick J., Terlevich R. J., 1999, *ApJ*, **519**, L123  
 Bellm E. C., et al., 2019, *PASP*, **131**, 018002  
 Bianchi S., Piconcelli E., Chiaberge M., Bailón E. J., Matt G., Fiore F., 2009, *ApJ*, **695**, 781  
 Caccianiga A., et al., 2008, *A&A*, **477**, 735  
 Chambers K. C., et al., 2016, *arXiv e-prints*, p. [arXiv:1612.05560](https://arxiv.org/abs/1612.05560)  
 Cohen R. D., Rudy R. J., Puetter R. C., Ake T. B., Foltz C. B., 1986, *ApJ*, **311**, 135  
 Denney K. D., et al., 2014, *ApJ*, **796**, 134  
 Drake A. J., et al., 2009, *ApJ*, **696**, 870  
 Eracleous M., Halpern J. P., 2001, *ApJ*, **554**, 240  
 Green P. J., et al., 2022, *ApJ*, **933**, 180  
 Guo H., Shen Y., Wang S., 2018, PyQSOFit: Python code to fit the spectrum of quasars, *Astrophysics Source Code Library*, record ascl:1809.008 (ascl:1809.008)  
 Hinkle J., 2022, *Transient Name Server Classification Report*, **2022-945**, 1  
 Jacobson-Galán W., Foley R., 2021, *Transient Name Server AstroNote*, **272**, 1  
 LaMassa S. M., et al., 2015, *ApJ*, **800**, 144  
 Lawrence A., 1987, *PASP*, **99**, 309  
 Li J., Wang Z., Zheng D., 2023, *MNRAS*, **522**, 2928  
 López-Navas E., et al., 2022, *MNRAS*, **513**, L57  
 López-Navas E., Arévalo P., Bernal S., Graham M. J., Hernández-García L., Lira P., Sánchez-Sáez P., 2023a, *MNRAS*, **518**, 1531  
 López-Navas E., et al., 2023b, *MNRAS*, **524**, 188  
 MacLeod C. L., et al., 2016, *MNRAS*, **457**, 389  
 Marchese E., Braitto V., Della Ceca R., Caccianiga A., Severgnini P., 2012, *MNRAS*, **421**, 1803  
 Matt G., Guainazzi M., Maiolino R., 2003, *MNRAS*, **342**, 422  
 McElroy R. E., et al., 2016, *A&A*, **593**, L8  
 Medford M. S., Lu J. R., Schlafly E. F., 2020, *Research Notes of the American Astronomical Society*, **4**, 38  
 Noda H., Done C., 2018, *MNRAS*, **480**, 3898  
 Pellegrino C., et al., 2022, *Transient Name Server Classification Report*, **2022-1070**, 1  
 Planck Collaboration et al., 2020, *A&A*, **641**, A6  
 Puccetti S., Fiore F., Risaliti G., Capalbi M., Elvis M., Nicastro F., 2007, *MNRAS*, **377**, 607  
 Ricci C., Trakhtenbrot B., 2022, *arXiv e-prints*, p. [arXiv:2211.05132](https://arxiv.org/abs/2211.05132)  
 Risaliti G., Young M., Elvis M., 2009, *ApJ*, **700**, L6  
 Ross N. P., et al., 2018, *MNRAS*, **480**, 4468  
 Ruan J. J., Anderson S. F., Dexter J., Agol E., 2014, *ApJ*, **783**, 105  
 Ruan J. J., et al., 2016, *ApJ*, **826**, 188  
 Shappee B. J., et al., 2014, *ApJ*, **788**, 48  
 Sheng Z., Wang T., Jiang N., Yang C., Yan L., Dou L., Peng B., 2017, *ApJ*, **846**, L7  
 Sheng Z., et al., 2020, *ApJ*, **889**, 46  
 Sniegowska M., Czerny B., Bon E., Bon N., 2020, *A&A*, **641**, A167  
 Stern D., et al., 2018, *ApJ*, **864**, 27  
 Storchi-Bergmann T., Baldwin J. A., Wilson A. S., 1993, *ApJ*, **410**, L11  
 Tadhunter C., 2008, *New Astron. Rev.*, **52**, 227  
 Tohline J. E., Osterbrock D. E., 1976, *ApJ*, **210**, L117  
 Tonry J. L., et al., 2018, *PASP*, **130**, 064505  
 Tozzi G., et al., 2022, *A&A*, **667**, L12  
 Urry C. M., Padovani P., 1995, *PASP*, **107**, 803  
 Vestergaard M., Peterson B. M., 2006, *ApJ*, **641**, 689  
 Wang C.-J., et al., 2019, *Research in Astronomy and Astrophysics*, **19**, 149  
 Wright E. L., et al., 2010, *AJ*, **140**, 1868  
 Yang Q., et al., 2018, *ApJ*, **862**, 109

## APPENDIX A: SPECTRUM FITTING WITH PYQSOFIT



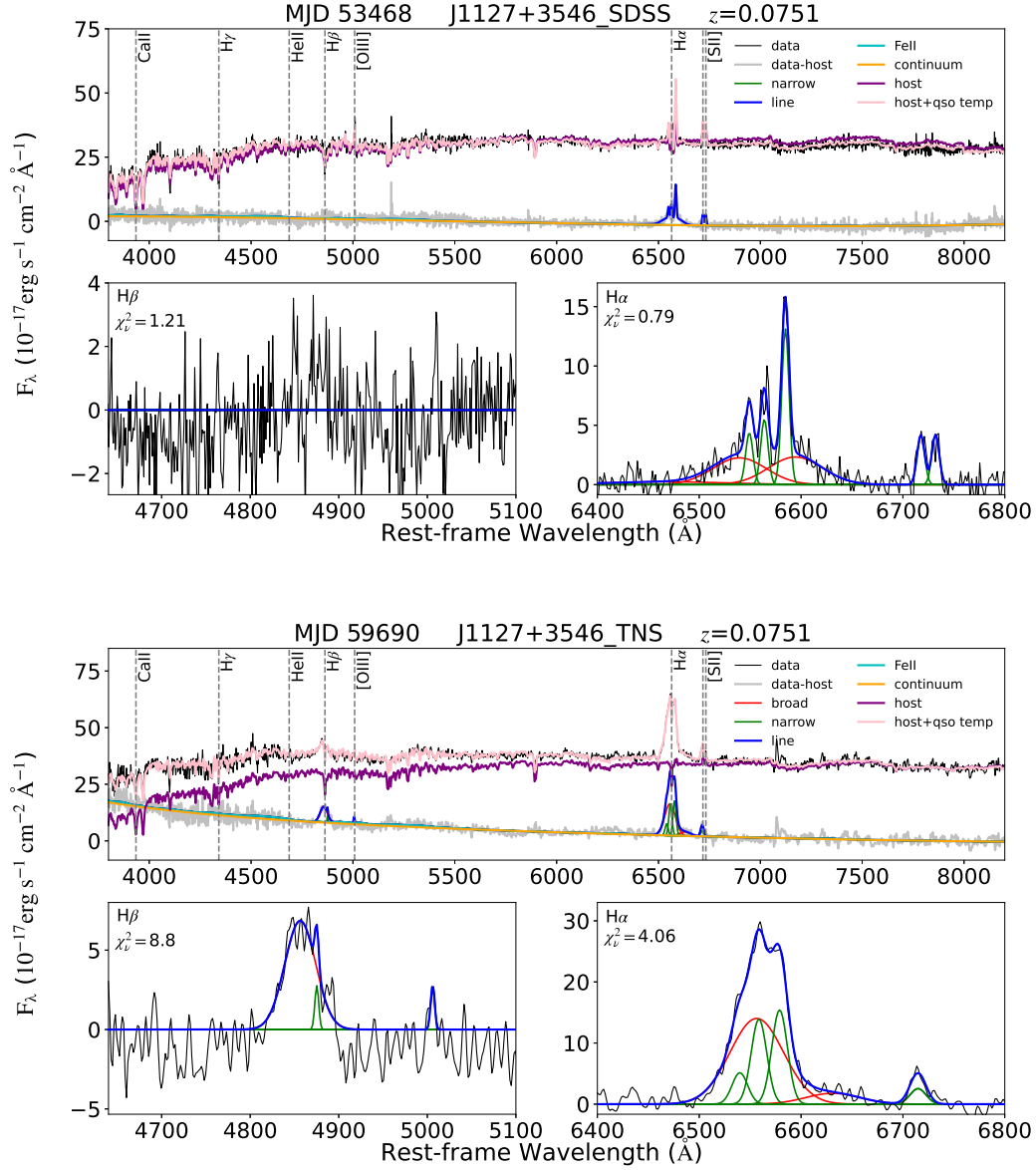
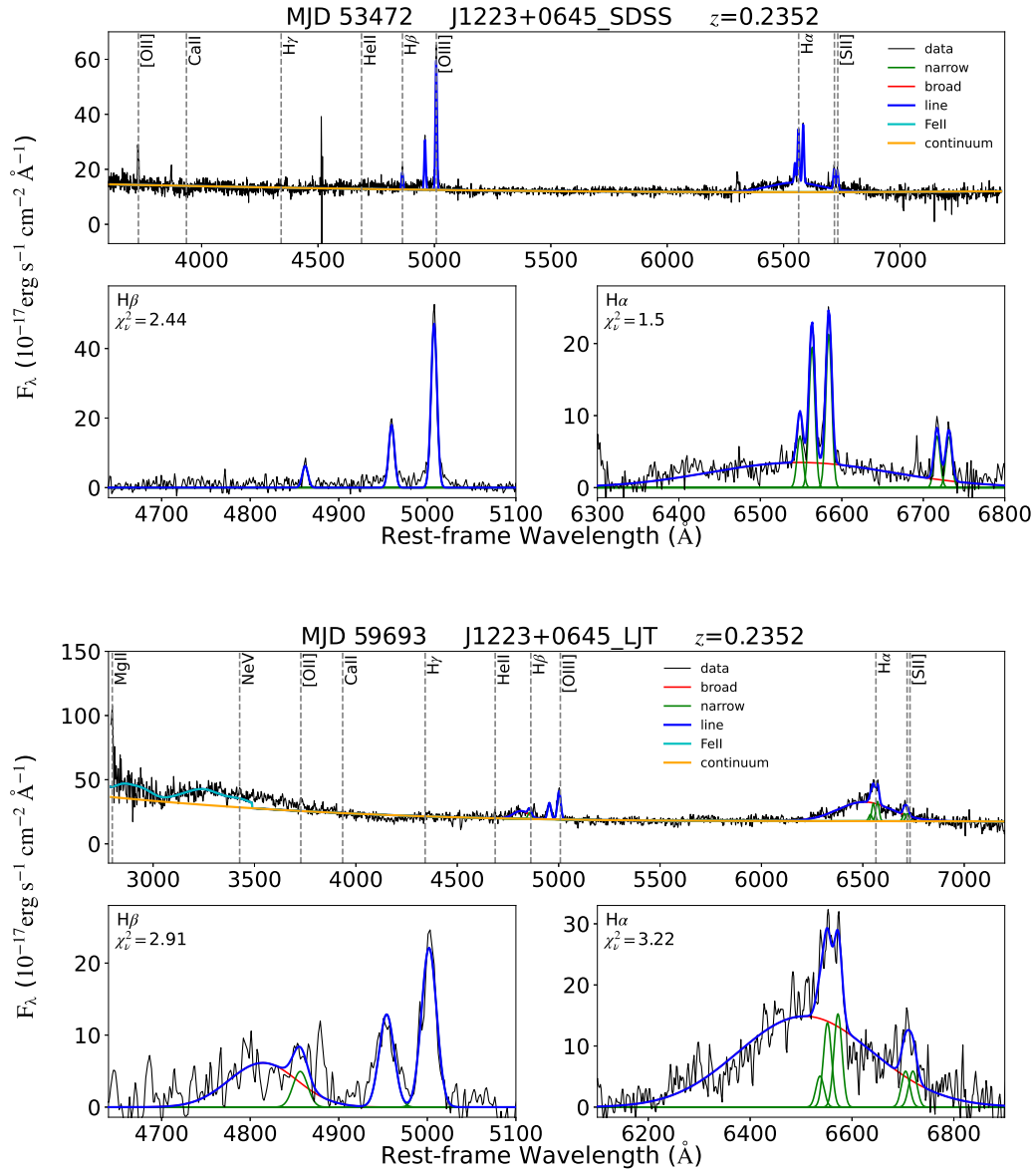


Figure A2. Spectral fitting for SDSS and TNS spectra of J1127+3546.



**Figure A3.** Spectral fitting for SDSS and LJT spectra of J1223+0645.

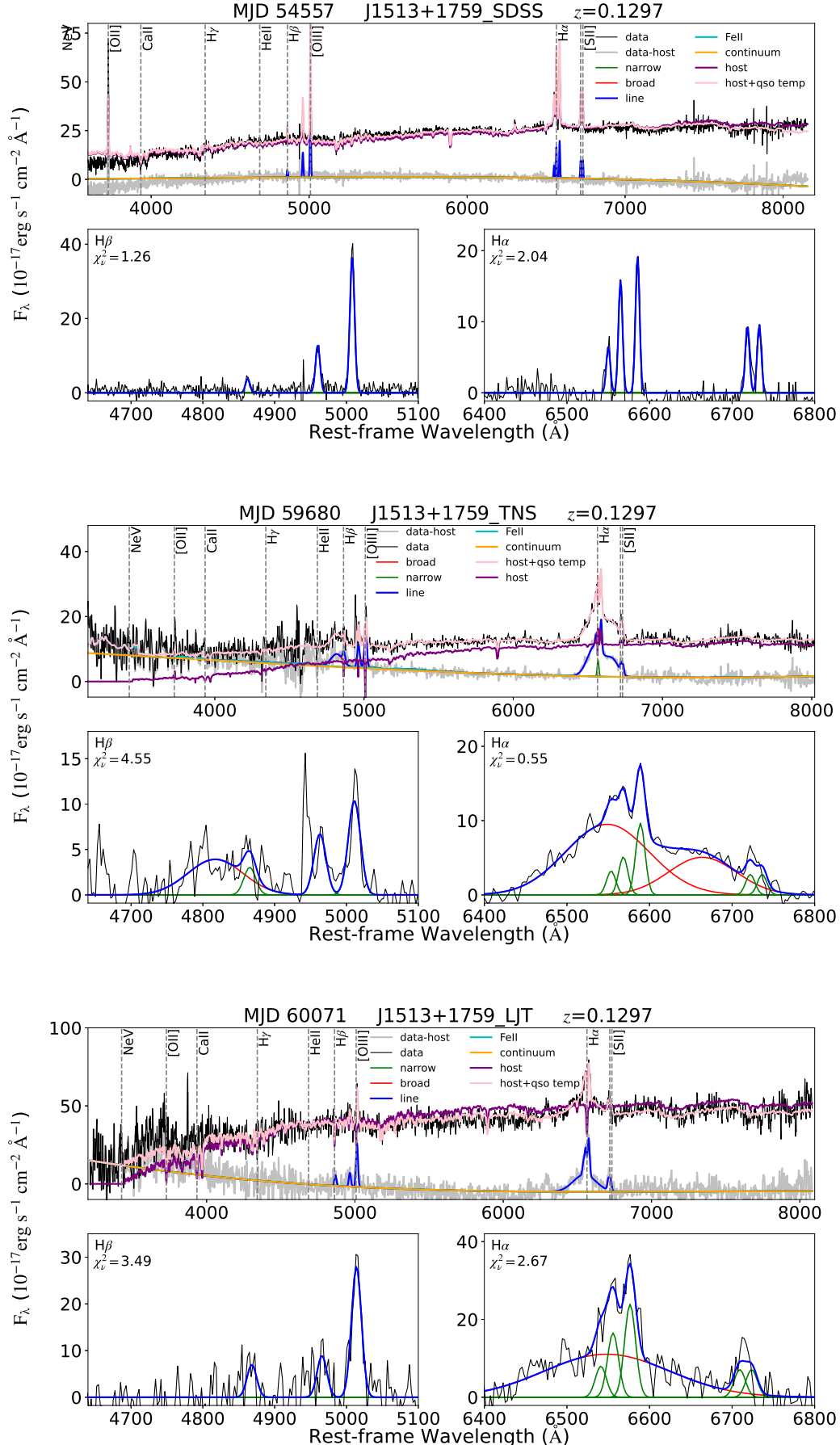
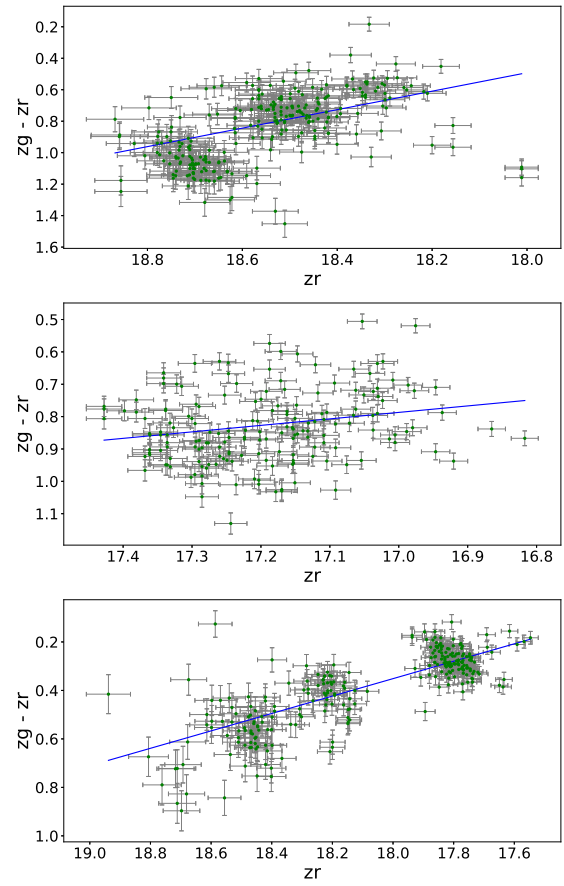


Figure A4. Spectral fitting for SDSS, TNS, and LJT spectra of J1513+1759.

**APPENDIX B: MAGNITUDE COLOR  
DIAGRAMS FOR THREE OF THE FOUR AGN**


**Figure B1.** Magnitude color diagrams for J0113+0135 (*top*), J1127+3546 (*middle*), and J1223+0645 (*bottom*). The  $z_g - z_r \propto k \times z_r$  fitting lines to the data points of the three sources are marked by a blue line in each panel, where  $k$  values are 0.59, 0.2, and 0.36, respectively.